



**HAL**  
open science

## Seasonal to decadal scale shoreline changes along the Cameroonian coastline, Bay of Bonny (1986 to 2020)

Njutapvoui Nourdi, Onguene Raphael, Abessolo Grégoire, Rudant Jean Paul,  
Bogning Sakaros, Thomas Stieglitz, Tomedi Minette

► **To cite this version:**

Njutapvoui Nourdi, Onguene Raphael, Abessolo Grégoire, Rudant Jean Paul, Bogning Sakaros, et al.. Seasonal to decadal scale shoreline changes along the Cameroonian coastline, Bay of Bonny (1986 to 2020). *Regional Studies in Marine Science*, 2021, 45, pp.101798. 10.1016/j.rsma.2021.101798 . ird-03219994

**HAL Id: ird-03219994**

**<https://ird.hal.science/ird-03219994>**

Submitted on 24 Nov 2021

**HAL** is a multi-disciplinary open access archive for the deposit and dissemination of scientific research documents, whether they are published or not. The documents may come from teaching and research institutions in France or abroad, or from public or private research centers.

L'archive ouverte pluridisciplinaire **HAL**, est destinée au dépôt et à la diffusion de documents scientifiques de niveau recherche, publiés ou non, émanant des établissements d'enseignement et de recherche français ou étrangers, des laboratoires publics ou privés.

# Regional Studies in Marine Science

## Seasonal to decadal scale wave induced shoreline changes along the Cameroonian coastline, Bay of Bonny (1986-2020)

--Manuscript Draft--

<b>Manuscript Number:</b>	
<b>Article Type:</b>	Research Paper
<b>Keywords:</b>	Coastline; wave climate; Bay of Bonny; optic; radar
<b>Corresponding Author:</b>	Nourdi Fokouop Njutapvou, M.D. Institute of Geological and Mining Research IRGM Yaounde, Centre CAMEROON
<b>First Author:</b>	Njutapvou F. Nourdi, M.D.
<b>Order of Authors:</b>	Njutapvou F. Nourdi, M.D. Onguéné Raphael, Dr Abessolo O. Grégoire, Dr Jean Paul Rudant, Pr Sakaros Bogning, Dr Thomas Stieglitz, Dr Tomedi E. Minette, Pr
<b>Abstract:</b>	The Bay of Bonny along the Cameroon coastline is home to diverse ecosystems. It is under substantial pressure from large human activity, but remains very little studied, like much of the Gulf of Guinea. In order to understand its long-term shoreline variations and the role the wave regime plays in the evolution of the coastline, a study was conducted on the basis of optical image archives from Landsat 5/7/8 and Sentinel-2A/2B satellite missions acquired between October 1986 and May 2020, coupled with daily ERA-Interim wave re-analysis data covering the period from January 1986 to August 2019. Overall, the results show that the evolution of the coast is highly variable in space and time, as indicated by different levels of erosion (30.55 %), and accretion (27.7 %) on the decadal-scale, with the most significant variations occurring in estuarine areas. Nevertheless, 41.75% of the Cameroon shoreline remains stable during the study period. Three main periods during which the coast underwent significant changes a different location were identified, reaching a retreat rate of up to -10 m/year in the northern section during 1986-1994. The wave regime decreases from the southern part towards the north, with an annual trend of significant wave heights of the five segments (-5.6 to -4.1 mm/year) with wave height maxima of $1.46 \pm 0.65$ m observed in the summer months (July-August). Monthly shoreline changes inversely correlated with the wave climate in some segments but are in line with the seasonal rhythm of the sub-region-s climate. The relatively strong local influence of erosion and accretion caused by natural dynamics (waves, drift currents) associated with the disproportionate presence of estuaries (Wouri, Rio del Rey, Sanaga) accounts for 76.3% of the observed variability, as indicated by analyses of eigenvalue orthogonal decomposition (mode 1, Empirical Orthogonal Functions).
<b>Suggested Reviewers:</b>	Dada A. Olusegun, Dr Lecturer, Federal University of Technology, Akure   futa oadada@futa.edu.ng he is one of the greatest authors and specialist in coastal dynamics in the Bay of Biafra area.  Edward Anthony, Pr European Center for Research and Education of Environmental Geosciences   CEREGEAix-Marseille University anthony@cerege.fr He worked on several themes including Response of the coast of the Gulf of Benin (Gulf of Guinea, West Africa) to anthropogenic and natural forcings.

Donatus Bapentire Angnuureng, Dr  
Centre for Coastal Management, University of Cape Coast, Ghana  
donatus.angnuureng@ucc.edu.gh

Rafael Almar  
Institut de recherche pour le developpement  
rafael.almar@ird.fr

August 17, 2020

Editor of **Regional Studies in Marine Science**

Dear Editor of **Regional Studies in Marine Science**

Please find enclosed our manuscript entitled “Seasonal to decadal scale wave induced shoreline changes along the Cameroonian coastline, Bay of Bonny (1986-2020)”. It presents understanding of coastline dynamics on country scale, the aim of this work is to study coastline variations over the last 34 years (1986 to 2020) and the role of wave climate in coastal changes in Bonny Bay (Cameroonian coast). We would like to submit this study to your journal as a research paper. We hope it fits the scope of the journal.

We are looking forward to hearing from you.

Kind regards,

Njutapvouï F. Nourdi on behalf of all the co-authors.

1  
2 1 Seasonal to decadal scale wave induced shoreline changes along the  
3  
4  
5 2 Cameroon coastline, Bay of Bonny (1986-2020)  
6

7 3 **Njutapvouï F. Nourdi<sup>1,4</sup>; Onguéné Raphael<sup>2</sup>; Abessolo O. Grégoire<sup>4</sup> ; Jean Paul Rudant<sup>3</sup>;**  
8  
9  
10 4 **Sakaros Bogning<sup>2,5</sup> ; Thomas Stieglitz<sup>6</sup> ; Tomedi E. Minette<sup>4</sup> ;**

11  
12  
13 5 <sup>1</sup> IRGM Institute of Geological and Mining Research; Vogt Street. BP: 4110 Yaoundé; Email:  
14  
15 6 njutapvouinourdi@yahoo.fr Phone: +237 656 05 49 14;

16  
17  
18 7 <sup>2</sup> Young Team Associated with IRD Response of the Cameroonian Coast to Multi-Scale Ocean  
19  
20 8 Forcing (JEAï-RELIFOME), University of Douala, BP 24 157 Douala, Cameroon;  
21  
22 9 ziongra@yahoo.fr

23  
24  
25 10 <sup>3</sup> LaSTIG/MATIS, Université Paris-Est, IGN, 5 Bd Descartes, Champs sur Marne, 77455 Marne  
26  
27 11 la Vallée CEDEX 2, France; rudant@univ-mlv.fr

28  
29 12 <sup>4</sup> Ecosystems and Fishery Resources Laboratory, Institute of Fisheries and Aquatic Sciences,  
30  
31 13 University of Douala, BP 2701 Douala, Cameroon.

32  
33  
34 14 <sup>5</sup> Département de Sciences de la Terre, Université de Douala, BP 24 157 Douala, Cameroun;  
35  
36 15 LEGOS Université de Toulouse, CNES, CNRS, IRD, UPS OMP, 14 Av. E. Belin, 31400 Toulouse,  
37  
38 16 France. Email: sakaros.bogning@legos.obs-mip.fr; Tel.: +33-561-332-970

39  
40  
41 17 <sup>6</sup> Marine Geophysical Laboratory, School of Mathematical and Physical Sciences, James Cook  
42  
43 18 University, Townsville QLD4811, Australia b Australian Institute of Marine Science,  
44  
45 19 Townsville QLD4810, Australia

46  
47  
48 20 Abstract

49  
50  
51 21 The Bay of Bonny along the Cameroon coastline is home to diverse ecosystems. It is under  
52  
53 22 substantial pressure from large human activity, but remains very little studied, like much of  
54  
55 23 the Gulf of Guinea. In order to understand its long-term shoreline variations and the role the

1 24 wave regime plays in the evolution of the coastline, a study was conducted on the basis of  
2  
3  
4 25 optical image archives from Landsat 5/7/8 and Sentinel-2A/2B satellite missions acquired  
5  
6 26 between October 1986 and May 2020, coupled with daily ERA-Interim wave re-analysis data  
7  
8  
9 27 covering the period from January 1986 to August 2019. Overall, the results show that the  
10  
11 28 evolution of the coast is highly variable in space and time, as indicated by different levels of  
12  
13 29 erosion (30.55 %), and accretion (27.7 %) on the decadal-scale, with the most significant  
14  
15 30 variations occurring in estuarine areas. Nevertheless, 41.75% of the Cameroon shoreline  
16  
17 31 remains stable during the study period. Three main periods during which the coast  
18  
19 32 underwent significant changes a different location were identified, reaching a retreat rate of  
20  
21 33 up to -10 m/year in the northern section during 1986-1994. The wave regime decreases  
22  
23 34 from the southern part towards the north, with an annual trend of significant wave heights  
24  
25 35 of the five segments (-5.6 to -4.1 mm/year) with wave height maxima of  $1.46 \pm 0.65$  m  
26  
27 36 observed in the summer months (July-August). Monthly shoreline changes inversely  
28  
29 37 correlated with the wave climate in some segments but are in line with the seasonal rhythm  
30  
31 38 of the sub-region-s climate. The relatively strong local influence of erosion and accretion  
32  
33 39 caused by natural dynamics (waves, drift currents) associated with the disproportionate  
34  
35 40 presence of estuaries (Wouri, Rio del Rey, Sanaga) accounts for 76.3% of the observed  
36  
37 41 variability, as indicated by analyses of eigenvalue orthogonal decomposition (mode 1,  
38  
39 42 Empirical Orthogonal Functions). These characteristics explain a complex pattern of  
40  
41 43 coastline changes with an almost continuous retreat shoreline during the period 1986-2012  
42  
43 44 and a reversal in trend towards accretion during the period 2012-2020. EOF mode 2 explains  
44  
45 45 23.7% of variability associated with the gradual overall decline from south to north over the  
46  
47 46 study period. This is attributed to an overall decrease in the supply of sediment via the  
48  
49 47 coastal transport system that prevails in the Gulf of Guinea.  
50  
51  
52  
53  
54  
55  
56  
57  
58  
59  
60  
61  
62  
63  
64  
65

1 48 **Key words:** Coastline, wave climate, Bay of Bonny, optic, radar  
2  
3

## 4 49 1. Introduction

5  
6  
7 50 Coastal areas around the world are increasingly anthropized and inhabited because of  
8  
9  
10 51 their socio-economic and recreational importance (Boateng, 2009, 2012). Several recent  
11  
12 52 studies (Luijendijk et al., 2018; Kuenzer et al., 2014; Dada et al., 2015, 2016) have shown that  
13  
14  
15 53 these environments are also subject to varying degrees of natural and anthropogenic  
16  
17 54 morphological variation, thereby increasing the vulnerability of these areas and the risks to  
18  
19  
20 55 property and people (Richards and Nichols, 2009). The very high vulnerability of some  
21  
22 56 coastal environments remains a major concern (Bosom and Jiménez, 2011; Tano et al. 2016)  
23  
24  
25 57 in view of the intensification of extreme wave and tidal events and sea level rise due to  
26  
27 58 climate change (Pilkey and Cooper, 2014; Ranasinghe, 2016; Anthony, 2017). Tropical  
28  
29  
30 59 coastal environments are particularly affected by erosion and flooding, but their variability  
31  
32 60 and vulnerability is still poorly understood, especially on long time scales (decades), due to  
33  
34  
35 61 the lack of adequate morphological and hydrodynamic data. Coastal management policies in  
36  
37 62 these regions are, more often than not, limited to local scale and not well informed to support  
38  
39  
40 63 sustainable coastal development on a large spatial scale.

41  
42 64 In West Africa, studies have been carried out on coastal zone dynamics to assess its  
43  
44  
45 65 vulnerability. Almar et al (2014) demonstrated the importance of understanding the causes  
46  
47 66 of erosion observed in the Bay of Benin on several scales, and Laibi et al. (2014)  
48  
49  
50 67 demonstrated the impact of the presence of ports and coastal infrastructures. The work of  
51  
52 68 Dada et al. 2016 has led to an understanding of the wave climate, its potential changes and  
53  
54  
55 69 its implications on coastal evolution for environmental monitoring and sustainable  
56  
57 70 management of the Niger Delta. In addition, several major projects have been launched in  
58  
59  
60 71 West Africa, including the West African Coastal Observation Mission (MOLOA, 2013), aimed  
61  
62  
63  
64  
65

1 72 at an integrated coastline management strategy, including the production of historical data  
2  
3 73 on coastal dynamics and risks in coastal areas. Giardino et al. 2018 proposed a large-scale  
4  
5 74 coastal policy for the development of sustainable management practices in coastal areas, but  
6  
7  
8 75 this is difficult to implement.  
9

10 76 Along the Cameroon coastline, few studies have been carried out on coastal dynamics.  
11  
12 77 Abessolo et al. 2018 have studied coastal erosion/accretion processes through the modelling  
13  
14 78 of barotropic currents in the Wouri estuaries in central Cameroon. The recent work of Fotsi  
15  
16 79 et al. 2019 on the temporal (1948-2012) and dynamic evolution of the Wouri estuary's  
17  
18 80 coastline have demonstrated the influence of the sedimentary regime on the variation of its  
19  
20 81 coastline. These works have shown that the Cameroonian coastline has undergone complex  
21  
22 82 patterns of shoreline modification. However, regional-scale sustainable coastal zone  
23  
24 83 management is hampered by a general lack of continuous and accurate historical data on the  
25  
26 84 position of the coastline. It is difficult to study the impact of hydrodynamic forcing on the  
27  
28 85 Cameroonian coastline due to the lack of morphological data. More importantly, the multi-  
29  
30 86 scale nature of wave impact: event-driven (impact of storms and waves, and tides); seasonal  
31  
32 87 (seasonal behaviour of the coastline); interannual to decadal trend (difficult to observe due  
33  
34 88 to lack of adequate data) remains almost unknown on this coast.  
35  
36  
37  
38  
39  
40  
41  
42

43 89 Given the current lack of data and understanding of coastline dynamics on country  
44  
45 90 scale, the aim of this work is to study coastline variations over the last 34 years (1986 to  
46  
47 91 2020) and the role of wave climate in coastal changes in Bonny Bay (Cameroonian coast).  
48  
49  
50

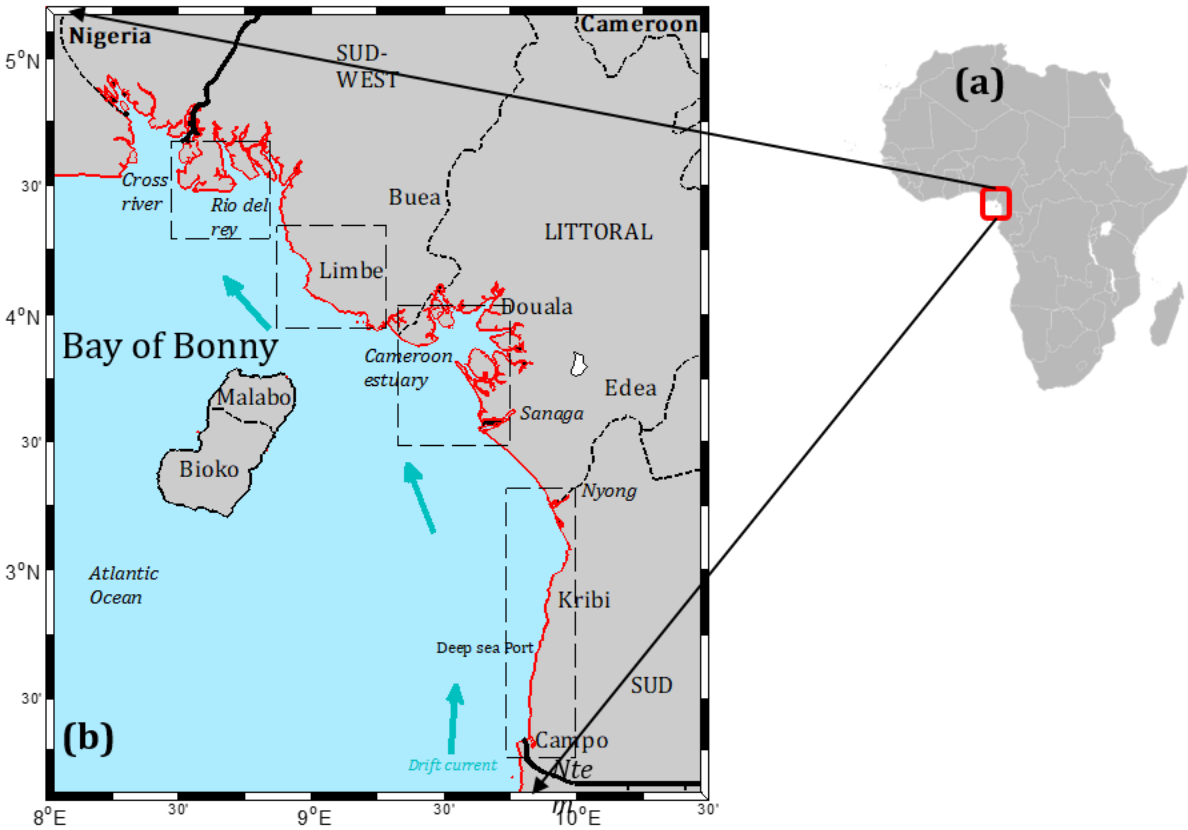
## 51 92 2. Materials and Methods

### 52 93 2.1. Study Site

53  
54  
55 94 The study area is located between Rio-del-Rey (Cameroon) to Campo (Equatorial  
56  
57 95 Guinea) and covers entire Cameroonian coastline in the Bay of Biafra (Fig. 1). This coast is  
58  
59  
60  
61  
62  
63  
64  
65

1 96 characterized by different ecosystems. Ten major rivers flow into the ocean, the most  
2  
3  
4 97 important of which are Ntem, Nyong, Sanaga, Wouri and the Rio del rey. Following Giresse  
5  
6 98 et al. (1996) four subsets (S-E) of the coast were defined (Fig. 1), as follows:  
7  
8  
9 99 - Subset 1: Composed of the Rio del rey and Cross river basins bordering the east of the Bakassi  
10  
11 100 peninsula in Cameroon, this complex is considered as an extension of the eastern zone of the  
12  
13 101 Niger delta set up during the Paleocene-Eocene. It contains the largest zone of mangroves  
14  
15 102 (125,259 hectares) in the country (Ajonina, 2010; MINEPDED-RCM, 2017) and a group of  
16  
17 103 islets. The Rio del Rey's estuary is open and shallow, with tidal amplitudes reaching up to 3  
18  
19 104 m.  
20  
21  
22  
23 105 - Sub-group 2 (Idenau to Limbé): This section is characterized by small basalt cliffs separated  
24  
25 106 by small bays with pebble and sand beaches on the volcanic base of Mount Cameroon.  
26  
27  
28 107 - Subset 3 (Cameroon estuary): with an area of 103,817 ha (ONEQUIP, 2009), it constitutes a  
29  
30 108 vast wetland, 30 km long and almost as wide; it is an integral part of the Wouri watershed.  
31  
32 109 The relief is formed by a succession of sedimentary plains. This bay is also bordered by the  
33  
34 110 second largest mangrove area (93,549 hectares) (MINEPDED-RCM, 2017), and is the  
35  
36 111 receptacle of the main rivers of the region (Wouri, Mungo and Dibamba). The average tidal  
37  
38 112 range is 2 m with maximum reaching 3 m in fast flowing waters. (Onguéné et al., 2015).  
39  
40  
41  
42  
43 113 - Subset 4 (Kribi-Campo): From the mouth of the Nyong to the Ntem River, this coast is  
44  
45 114 characterized by the presence of sandy beaches, which alternate with rocky headlands,  
46  
47 115 lagoons, mangroves and other coastal vegetation. It contains two protected areas (Douala-  
48  
49 116 Edea Wildlife Reserve and Campo-Ma'an National Park). The tidal range is about 1.8 m at  
50  
51  
52  
53  
54  
55  
56  
57  
58  
59  
60  
61  
62  
63  
64  
65

1 117 Campo, 1.5 m at Kribi and 1.2 m at Petit-Batanga. (Giresse et al., 1996).



118  
119 Figure 1: The coast of Cameroon in Bay of Bonny. The study area extends from the mouth of  
120 the *Ntem* (border with Equatorial Guinea to the south) to the Rio del Rey at the Nigerian  
121 border. This mesotidal coast is dominated by waves and regional current that generate a  
122 strong S-SW longshore drift. The three main cities of the coast, Kribi, Douala and Limbe, are  
123 each presented in the figure b.

## 124 2.2 Landsat and Sentinel-2 Image Extraction and Processing Under DSAS

125 We extracted a set of 10 images with less than 10% cloud cover (a common problem in  
126 the tropics), i.e. 7 images from Landsat 5/7/8 missions downloaded from  
127 earthexplorer.usgs.gov and 3 images from the Sentinel 2A/2B satellites downloaded from  
128 the Copernicus platform (<https://scihub.copernicus.eu/dhus/>) of the ESA (European Space  
129 Agency). All Landsat satellites are orbiting at an altitude of 705 km with a swath of 185 km  
130 / 185 km (Fernand, 2002). The "Sentinel-2" constellation, on the other hand, consists of two

1 131 satellites (Sentinel-2A and Sentinel-2B), at an altitude of 786 km and a swath of 250/250 km.  
 2  
 3  
 4 132 Orbiting on the same sun-synchronous trajectory, but with a phase shift of 180° with respect  
 5  
 6 133 to each other. The revisit time is 10 days for each satellite (Tab. 1), which corresponds to 5  
 7  
 8  
 9 134 days for the couple S-2A and S2-B. A summary of the different characteristics of the images  
 10  
 11 135 is given in Table 1.

14 136 Table 1: Summary of the satellite images used in this study.

Satellite Mission	sensors	Revisit period	Pixel size and band used	Acquisition date (yyyy/mm/dd)	Cloud cover(%)	Number of images
Landsat 5	TM		30 m, Bands: R (B3), G (B2), B (B1) NIR (B4), SWIR1 (B5, B7)	1986/01/26	3.6	1
Landsat 7	ETM+	16 days	30 m, Bands: R (B3), G (B2), B (B1) NIR (B4), SWIR1 (B5, B7) +15 m panchromatic band	1999/12/17 2005/03/27 2010/02/14	2.4 6.2 1.24	3
Landsat 8	OLI		30 m, Bands: R (B3), G (B2), B (B1) NIR (B4), SWIR1 (B5, B7) +15 m panchromatic band	2013/12/22 2016/03/27 2018/02/03	5.14 1.33 6.31	3
Sentinel 2A/2B	MSI	5 days (Couple S-2A and S-2B)	10 m Bands: R(B4), G(B3), B(B2) NIR (B8) +20 m SWIR1 (B12, B11)	2015/11/29 2017/05/07 2020/05/26	5 2.42 0.97	3

31  
 32  
 33 138 *TM (Thematic Mapper), ETM+ (Enhanced Thematic Mapper), OLI (Operational Land Imager),*  
 34  
 35 139 *MSI (Multi-spectral instrument); R: red, G: green, B: blue, NIR: near infrared, SWIR: short wave*  
 36  
 37  
 38 140 *infrared. B1-B12: spectral bands.*

39  
 40  
 41 141 A series of digital pre-processing was carried out on all the images, ranging from geo-  
 42  
 43 142 referencing, resetting the images of the various sensors, atmospheric and radiometric  
 44  
 45 143 correction, contrast enhancement, and the application of a cloud mask to eliminate all images  
 46  
 47 144 that exceed a certain percentage of cloud cover (include a reference that describes this  
 48  
 49 145 approach). The quality of the satellite images was improved to obtain optimal detection of  
 50  
 51 146 the coastline by pan-sharpening (combining the visible band (30 m for Landsat and 10 m for  
 52  
 53 147 Sentinel 2) with the panchromatic band (15 m for Landsat and 10 m for Sentinel). After this  
 54  
 55 148 step, all bands were reduced to 15 and 10 m for the pixel size of Landsat 7&8 and Sentinel  
 56  
 57  
 58  
 59  
 60  
 61  
 62  
 63  
 64  
 65

1 149 2A/B respectively, in order to obtain images with better image quality while decreasing as  
2  
3  
4 150 much as possible the digital precision error.  
5  
6 151 Subsequently, image mosaics were created in order to obtain overall images of the study  
7  
8  
9 152 area. A coloured composition of the bands of each sensor was performed (Tab. 1 column 3),  
10  
11 153 in order to choose the most appropriate channel to extract the indicator used as a coastline  
12  
13 154 marker (Robin, 2002). Classically, shoreline detection is carried out either in the near  
14  
15  
16 155 infrared or mid-infrared due to the low reflectance of water in the infrared range of the  
17  
18 156 electromagnetic spectrum. On this basis, in order to best highlight the contact between the  
19  
20  
21 157 dry sediments of the high beach and the vegetation cover a coloured composition of the  
22  
23 158 spectral bands was therefore used to discriminate the high beach/vegetation interface  
24  
25  
26 159 (Robin, 2002).

27  
28  
29 160 To calculate and map the overall coastline displacement rate, the Digital Shoreline  
30  
31 161 Analysis System (DSAS) plug-in version 4.3 (Thieler et al., 2009), in ArcMap software,  
32  
33 162 shoreline detection and extraction was performed manually by scanning the visible  
34  
35  
36 163 vegetation line and using 1986 as the baseline, the rates of shoreline change for 1999, 2005,  
37  
38 164 2010, 2013, 2015, 2016, 2017, 2018, and 2020 were calculated. All extracted coastlines were  
39  
40  
41 165 projected to the World Geodetic System UTM 32N reference system (WGS 84). After selecting  
42  
43 166 the 1986 reference line (baseline), the transects were projected from this line at 500 m  
44  
45  
46 167 intervals which intercepted each coastline initially vectorised. The Net Shoreline Motion  
47  
48 168 (NSM) and End Point Rate (EPR) statistics incorporated in DSAS were calculated to estimate  
49  
50  
51 169 the shoreline variation for the entire study period. We also specified for each coastline a  
52  
53 170 global uncertainty value (+/- 15 m) which accounts for the positional and measurement  
54  
55  
56 171 uncertainties.

### 2.3. Landsat and Sentinel-2 image extraction and processing with the CoastSat Toolbox

In order to obtain a longer and less constraining time series, to study the across-shore variability of the coastline, we used a stack of 425 images retrieved from the Google Earth Engine (GEE) platform via the open-source CoastSat toolkit (Python version 3.6), that allowed us to obtain time series of shoreline position with a horizontal accuracy of 10 m any sandy coastline worldwide (Vos et al., 2019). This algorithm allows to retrieve TOA (Top-of-Atmosphere) reflectance images from the GEE archives of Landsat 5/7/8 and Sentinel-2 satellites; and subsequently perform pre-processing of multi-spectral images (cloud masking, pan-sharpening, classification) as described in (Vos et al., 2019). Unlike DSAS, the Coastsat toolbox performs an automatic extraction from a single reference line (baseline) digitized by the user. It then generates the line for each of the sub-pixel resolution images (van der Walt et al., 2014). However, the results only become usable after applying a tidal correction (Eq. 2), which is not implemented in the toolbox as it is specific to each area (Vos et al., 2019). The user has the option of choosing a profile in which the time series of the cross-shore distance along the user-defined normal coastal transects is generated.

### 2.4 Estimation of errors associated with the position of the coastline

To constrain coastline change rates, we estimated four sources of error based on the method of Hapke et al. 2010, i.e. uncertainties associated with georeferencing, digitization, satellite position and tidal water level uncertainty. The mean values for each uncertainty term are presented in Table 2.

The error in digitizing the coastline depends on several factors including the quality of the reference data; the accuracy of the digitization (operator application); the expertise of the operator in interpreting the reference data.

1 195 Following Moore and Griggs (2002), the total error related to digitizing (Eq. 1) can be  
 2  
 3  
 4 196 estimated by the sum of the mean ( $\bar{X}$ ) of the offsets recorded during the repetition of the  
 5  
 6 197 digitization and 2 standard deviations ( $2\sigma$ ) :

$$- E_d = \bar{X} + 2\sigma \quad (1)$$

11  
 12 199 To obtain the errors related to tidal sea level oscillations, it is recommended that along coasts  
 13  
 14  
 15 200 with large tidal ranges and/or flatter beach profiles, all shorelines be adjusted to a standard  
 16  
 17  
 18 201 reference elevation (Stafford and Langfelder, 1971). Since all images are acquired between  
 19  
 20 202 09:00 and 10:00 local time, but at different stages of the tide, a linear tidal correction can be  
 21  
 22  
 23 203 applied using the measured water levels and the characteristic beach slope to translate each  
 24  
 25 204 shoreline into a reference elevation as follows:

$$E_t = \frac{(Z_{ref} - Z_{wl})}{\tan\beta} \quad (2)$$

26  
 27  
 28  
 29  
 30 205  
 31  
 32 206  $E_t$  is the horizontal offset across the normal transect to the coast,  $Z_{ref}$  is the reference  
 33  
 34  
 35 207 elevation (e.g. 0 m above mean sea level) and  $Z_{wl}$  is the local water level at the time of image  
 36  
 37 208 acquisition, and  $\tan\beta$  is the beach slope. The precise time of image acquisition to obtain the  
 38  
 39  
 40 209 local water level is stored in the image metadata.

41  
 42 210 Field work carried out on the beaches of the southern part of Cameroon (Kribi) showed  
 43  
 44  
 45 211 that the typical average slope  $\tan\beta$  is 0.57 or (5.7%). The significant wave height (Hs)  
 46  
 47 212 provided by ERA-Interim shows an overall average of 1.04 m off the coast. Tide levels remain  
 48  
 49  
 50 213 relatively low ( $\leq 2$  m). Thus, for example, the Landsat 8 image of 06 June 2013 was recorded  
 51  
 52 214 at 09 h 41 min coinciding with a tidal level of 0.4 m. The error (Eq.3) is considered here as  
 53  
 54  
 55 215 the sum of the squares of the different sources of error mentioned above:

$$E_i = E_g^2 + E_t^2 + E_d^2 + E_p^2 \quad (3) ; E_i \text{ error of time period } i \{1,2,\dots,n\}$$

$$ET = \sqrt{(E_{i1}^2 + E_{i2}^2 + E_{i3}^2)} \quad (4) E_T \text{ error for each period}$$

$$EA = \frac{\sum ET}{T_2 - T_1} \quad (5) EA : \text{annual error ; T time difference}$$

Table 2: Estimated errors calculated during data processing.

Measurement errors	Uncertainty (m) 1986-2020			
	Landsat 5	Landsat 7	Landsat 8	Sentinel 2
Georeferencing error (Eg)	5	2.5	2.5	1
Digitizing error (Ed)	± 1.5	1.05	1.05	0.7
Tide error (Et)	/	5.24	4.28	2.04
Pixel size error (Ep)	30	15	15	10
Totat shoreline position error (ET)				18.16
Annualize Error (EA)				0.55

## 2.5. In-situ data and processing

Given the near absence of field data on the coast, daily topographic survey campaigns using theodolite and GPS were carried out between 09-30 April 2018 in the Kribi area (C5), and between 13-31 May 2019 for the Limbé area (C2). Data was recorded at low tide in order to set the reference height Z=0 with respect to the mean sea level. We performed a resetting and georeferencing in a Mercator WGS84 projection system with an absolute planimetric accuracy of less than 5 m. This was done in order to bring all the data into the same geographic coordinate system as the satellite data. An instantaneous long-shore and cross-shore average over a 100 m interval was necessary to reduce the error of the coastline position during the survey.

## 2.6. Extraction and processing of Era-Interim wave data

Wave parameters (significant height Hs, period Tp and direction) were extracted from the server of the European Centre for Medium-Range Weather Forecasts (ECMWF/ECMWF

234 <https://apps.ecmwf.int/datasets/data/interim-full-daily/>) on a 0.125° x 0.125° grid, with a  
 235 time delay of one day resolution, from January 1986 to August 2019. These data are part of  
 236 the ERA-Interim dataset from the Ers-1&2, Envisat, Jason-1&2 altimetry missions, which  
 237 involves the analyses of global meteorological variables (Dee et al., 2011; Sterl and Caires,  
 238 2005). These data have been widely validated against buoys and altimetry data (Sterl and  
 239 Caires, 2005), with maximum wave height ( $H_s > 5\text{m}$ ) and minimum wave height ( $H_s < 1\text{m}$ )  
 240 tending to be under and overestimated respectively (Caires, Swail and Wang., 2006).  
 241 Fortunately, extreme wave conditions are generally not observed in the relatively constant  
 242 wave regime in the Gulf of Guinea.

243 We extracted the time series of  $H_s$  for the grid points closest to the coast and then used  
 244 time averages of the wave parameters for each segment (C1 to C5) over a period of 33 years.  
 245 However, as larges do not reach the Cameroonian coast, we used the formula proposed by  
 246 Larson et al in 2010 (Eq. 5) to calculate  $H_s$ ,  $T_p$  and direction at the closest grid point to the  
 247 coast. This method has been validated by the properties of deep-water waves (Larson et al.,  
 248 2010).

$$249 \quad h_b = (\lambda C^2)/g; \quad (5)$$

$$250 \quad \alpha_b = \text{asin}(\sin(\alpha_0 \sqrt{\lambda})) \quad (6)$$

251 Avec  $\lambda = \Delta \lambda_\alpha$ ; considering

$$252 \quad \Delta = 1 + 0.1649\xi + 0.5948\xi^2 - 1.6787\xi^3 + 2.8573\xi^4 \quad (7)$$

$$253 \quad \xi = \lambda_\alpha \sin^2 \theta_0; \lambda_\alpha = [\cos(\alpha_0)/\theta]^{2/5}; \theta = \left(\frac{c}{\sqrt{gH}}\right)^4 \left(\frac{c}{c_g}\right) \gamma^2 \quad (8)$$

254  $h_b$  wave height at wave break;  $T$  period (does not change as it propagates from the open sea  
 255 to the coast);  $\gamma = h_b/H$  wave breaking threshold following Battjes and Janssen (1978)  $H$

1 256 depth at the point of wave breaking, and finally  $C_g = C/2$  the group velocity of waves  
2  
3  
4 257 propagating towards the coast and  $\theta_0$  and  $\theta$  direction of waves in deep water and at the point  
5  
6 258 of wave breaking respectively.

9 259 We averaged each series of data (coastline and Hs) on a monthly basis for each  
10  
11 260 segment. Subsequently, a mean value was calculated and subtracted from each value in the  
12  
13  
14 261 data series. Seasonal signal were removed, using a least square fit to the sine functions,  
15  
16 262 before calculating trends. The trend calculation was based on a simple linear regression fit.

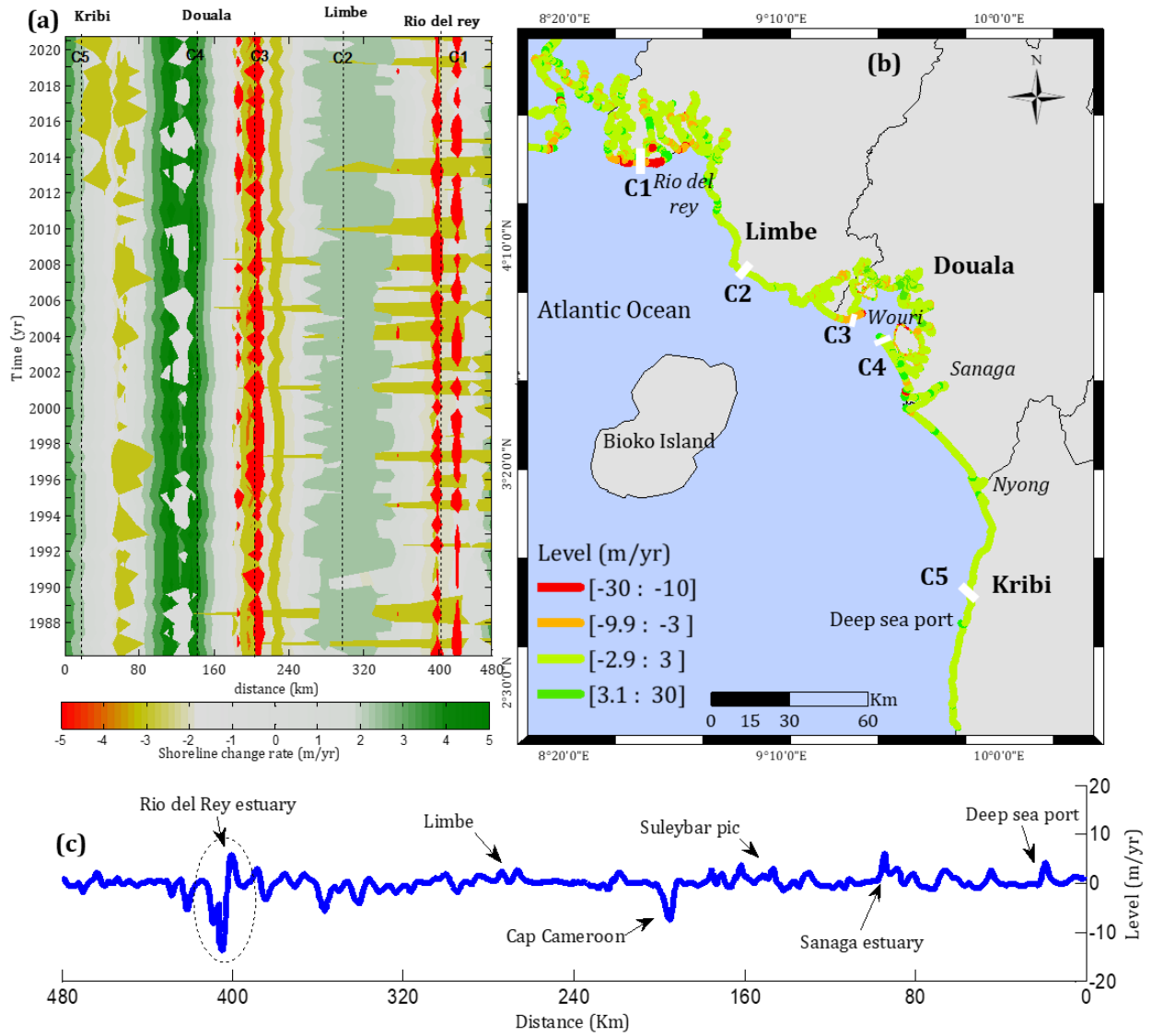
19 263 -  $f(x) = a_n * \sin(b_n * x + c_n)$   $n \in \mathbb{N}$  (9)

22 264 With a amplitude; b angular speed and c the phase shift.

## 265 3 Results

### 266 3.1 Coastal changes from 1986 to 2020

31 267 DSAS analyses indicate that 30.55% of Cameroon's shoreline are eroding, 27.70% are  
32  
33 268 accreting and 41.75% are stable. Figure 2c illustrates the longshore variation of the coastline  
34  
35  
36 269 during the period 1986 to 2020 following a period marked by deep and permanent changes  
37  
38 270 in the estuaries (C1 and C3) of the Rio del Rey and Wouri estuaries respectively. Some areas  
39  
40  
41 271 were found to be stable (C2, Limbe), and some areas with small-scale shoreline changes were  
42  
43 272 identified. e.g. C5 (Kribi Coast) with erosion and deposition rates ranging between -2.7 and  
44  
45  
46 273 2.1 m/year, and only a minor displacement of the shoreline of 10 m between 2008 and 2013  
47  
48 274 observed on the northern coast of Kribi (Fig.2a). The maximum observed erosion occurred  
49  
50 275 at Rio del rey and Cap Cameroon (C3) with significant shoreline retreats of up to -19.2 /year.



276  
277 Figure 2 Map of spatio-temporal changes showing erosion/accretion evolution. (a)  
278 Hovmoller diagram rate of change; (b) Overall coastline placement rate with sub-areas of  
279 interest identified (transects: white dash C1 to C5); (c) Net rate of shoreline change between  
280 1986-2020 showing a linear velocity trend along the coastline.

281 Table 3 shows small changes (between 0.43 and 0.65 m/year) in the Kribi (C5) and  
282 Limbé (C2) segment. Significant and very localised changes are observed with an erosion of  
283 -11 to -6 m/year respectively in C1 and C3. Section (see above on section, part, segment...)

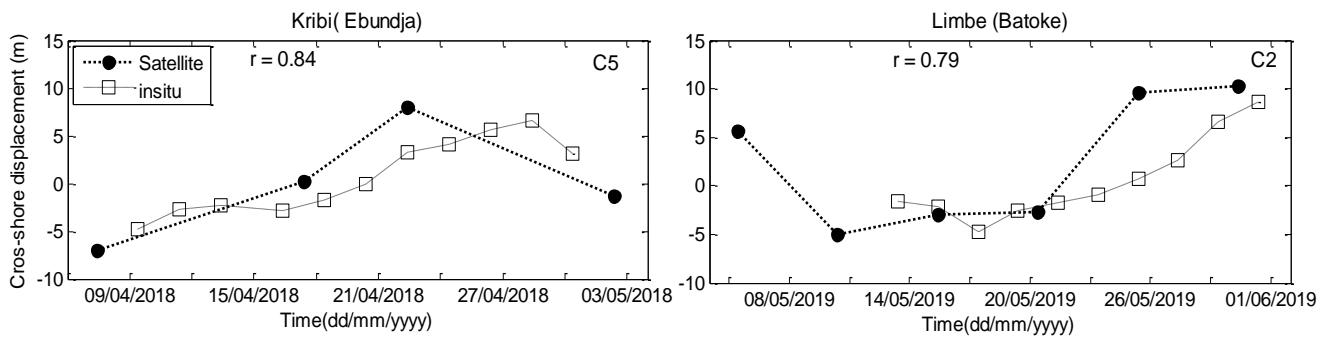
284 C4 is accumulating while parts C1 and C3 are heavily eroding. An illustration is made by the  
 285 diagram in figure 2a, which shows permanent erosion well before the year 1988.

286 Table 3: Area change and overall observed displacement rate by area of interest

	Kribi (C5)	Suleybar pic (C4)	Cap Cameroon (C3)	Limbe (C2)	Rio del rey (C1)
Surface (km <sup>2</sup> )	11.5	8.21	6.4	8.24	25.87
Displacement rate (m/yr)	0.65 ± 0.04	5.87 ± 0.78	-6.05 ± 1.43	0.43 ± 0.05	-11.601 ± 4.02
Observation (1986-2020)	Stable	strong accretion	erosion	weak accretion	strong erosion

### 3.2 Validation of coastline positions derived from satellite imagery with in-situ measurements

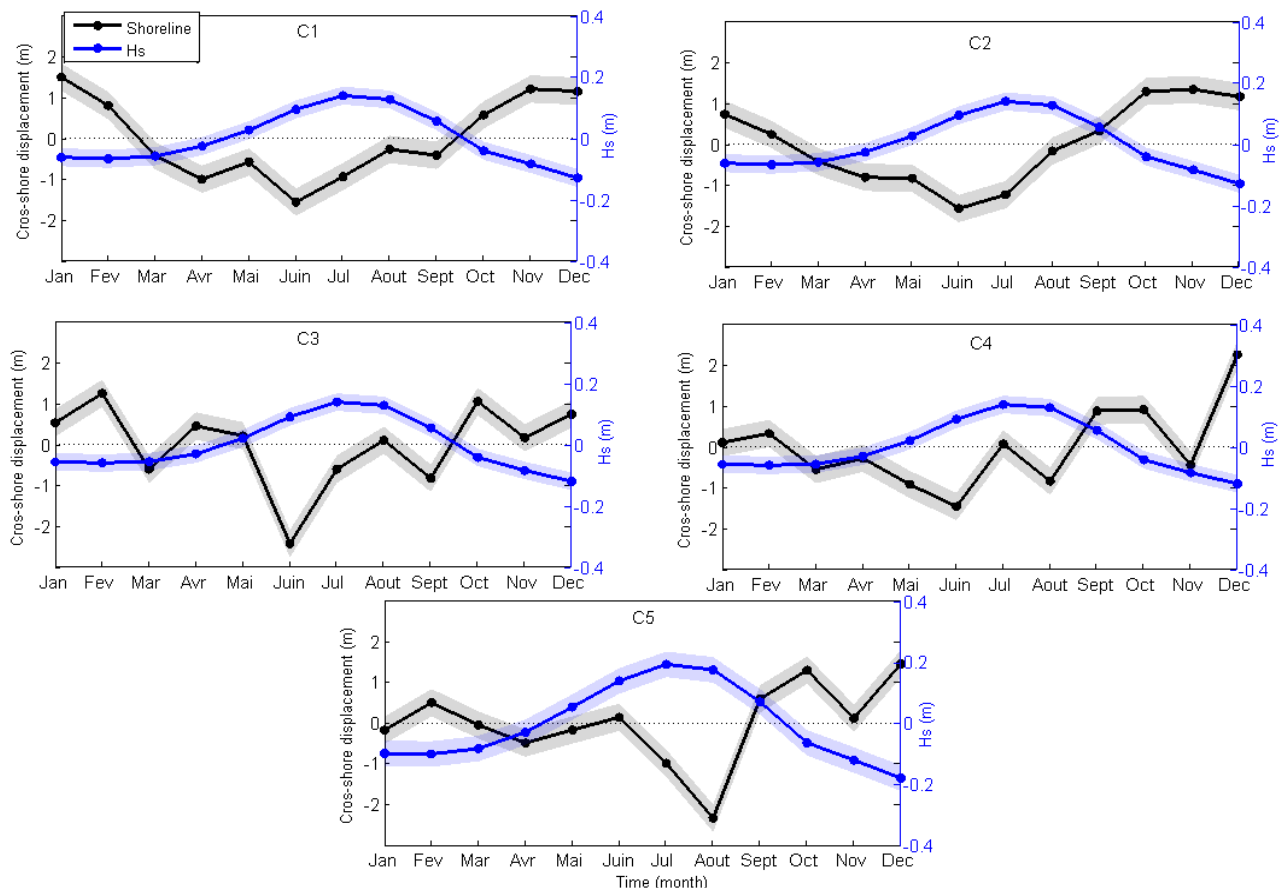
To ground-truth satellite-based data, satellite-derived results were compared with field data at C2 and C5 (Fig. 3). Data from other sections are not available. The comparison indicates that the satellites are able to well identify the main horizontal coastline changes ( $r = 0.84$  for C5 and  $0.79$  for C2).



294 Figure 3: difference in across-shore displacement between in situ and satellite  
 295 measurements (Kribi C5 and Limbé C2).  
 296

### 3.3 Seasonal coastline variability and wave regime

The results of the seasonal analysis of shoreline changes and waves are shown in Figure 4. It is noted that the seasonal variation of the shoreline presents two different phases, an accretion phase in winter (September to February) and an erosion phase in summer (March to August). During this later phase, the maximum erosion is reached in June except in C5 where the maximum is reached in August ( $-2 \pm 0.32$  m). The wave regime is characterized by summer waves with a significant monthly mean height between 1.2 m and 1.7 m respectively in segments C1 and C5. Summer Hs are highest near C5 and lowest at C1 to C2 (northern part). It is during periods of high turbulence that significant erosional disturbance of the shoreline is observed. Note that a delay is generally observed between high Hs values and shoreline movement. During the winter (September to February), Hs values are almost below the annual average in all segment. (Fig. 4).



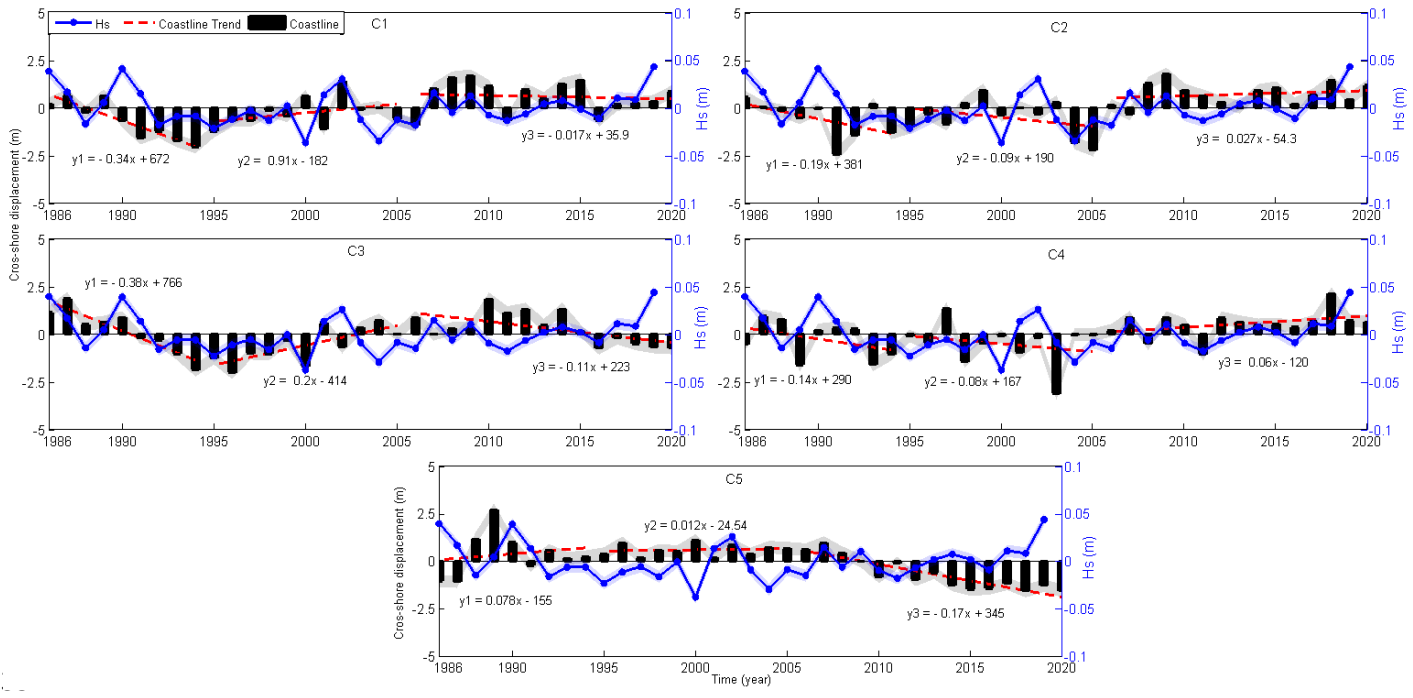
309

1 310 Figure 4: Monthly variation in coastline and waves by segment (C1 to C5). Mean values and  
2  
3  
4 311 uncertainties ( $\pm$  standard deviation) are shown. The monthly coastlines are derived from the  
5  
6 312 processing of the 425 GEE archive images via the CoastSat Toolbox. The blue curve  
7  
8 313 represents the monthly variation in wave height, while the black curve represents the  
9  
10 314 monthly coastline changes during the period 1986-2020.

### 14 315 3.4 Interannual coastline and wave height variability

16 316 Interannual analyses (fig. 5) show significant fluctuations of the coastline from one year to  
17 317 another and from one site to another. The interannual evolution of the coastline shows three  
18  
19 318 main periods of significant change from one segment to another. In segment C1, there was a  
20  
21 319 marked retreat of the coastline during the first period (1986-1994), of the order of  $-3 \pm 1.4$   
22 320 m. Hs peaked in 1990 and subsequently declined with a trend of  $-0.0047$  m/year. Significant  
23  
24 321 accretion shifts began to occur in the second period (1994 to 2005). In the final period the  
25  
26 322 shoreline oscillated between erosion and accretion. In C2, the first two periods are marked  
27  
28 323 by a regressive trend of the order of  $-4 \pm 0.2$  m, followed by a period of accretion during the  
29  
30 324 third period (2006-2020). Segment C3 is marked by a pronounced shoreline retreat of  $-9.4$   
31  
32 325  $\pm 0.7$  m over the 1986-1996 period. As in C1, the second period shows an accretion trend of  
33  
34 326  $0.8 \pm 0.0021$  m/year, followed by a period of erosion (1994-2005). Segment C4 is relatively  
35  
36 327 stable with time, marked by some punctual periods of erosion and accretion. In C5 a  
37  
38 328 maximum interannual progradation of the coastline of  $10 \pm 1.45$  m was reached in 1989  
39  
40 329 followed by a long period of average stability of  $0.76 \pm 1.3$  m (1992-2007). A continuous  
41  
42 330 regression of the order of  $-5 \pm 0.23$  m was observed during the period 2008 to 2015. Linear  
43  
44 331 regression analysis for shoreline changes from 1986 to 2020 showed a general erosion trend  
45  
46 332 of  $\sim -6.2$  m/year during the first period (1986-1994) and accretion trends during the second  
47  
48  
49  
50  
51  
52  
53  
54  
55  
56  
57  
58  
59  
60  
61  
62  
63  
64  
65

1 333 period of 2.4 m/year (Fig.5). The final period is dominated by low-scale erosion of the order  
 2  
 3  
 4 334 of  $-1.3 \pm 0.75$  m.



3 335  
 28 336 Figure 5. Interannual coastline and wave variability by segment (C1 to C5). The coastline  
 31 337 trend is represented by the red line; uncertainties are also associated with the curves ( $\pm$   
 32 338 standard deviation). These results are derived from the processing of the 425 GEE archive  
 35 339 images via the CoastSat Toolbox.

40 340 The interannual variation of waves in each segment (C1 to C5) shows a weak and  
 42 341 constant wave climate distribution ( $T_p = 7$  to  $12$  s in S-SW direction), the annual mean of Hs  
 44 342 varies from  $0.7$  to  $1.7$  m with maximum of  $1.7 \pm 0.12$  mm in C5. The interannual wave  
 47 343 variability Fig 5 (C1-C5), shows an overall decrease in height during the first period of 1986  
 49 344 - 1994 with an annual downward trend at all segments ( $-0.0056$  to  $-0.0041$ m/year). Despite  
 52 345 a significant fluctuation observed between 1999-2001, the second period (1995 to 2005) is  
 54 346 marked by a relative stability in wave heights (trend between  $0.0002$  and  $0.0006$  m/year)  
 57 347 on the whole coast. The third period (2006 - 2019) is characterized by annual upward trends  
 59 348 of Hs ( $0.0017$  to  $0.003$  m/year) with an amplitude that increases towards the south (i.e. from

segment C1 to C5). Distinct peaks characterized by values of Hs above the annual average as shown in Figure 5 (C1 to C5), were observed in 1986, 1990, 2002 and 2019.

Interannual coastal changes were correlated to wave climates and the results are shown on Table 4. The variability of wave climate is more correlated with the coastline dynamics during the first period (1986-1994), with a correlation coefficient  $r = 0.5$  in segments C1 to C4. While between 2005 and 2020, the wave regime could be responsible for the erosion observed at C3 ( $r = -0.65$ ). Overall, these results indicate that waves do not fully explain the high variability along the coastline. However, the involvement of waves makes it possible to understand more than 40% of the coastline dynamics in certain segments.

Table 4: correlation coefficients between coastline and wave trend at interannual scale.

Corrélation $\Delta X$ & Hs	Kribi (C5)	Suleybar pic (C4)	Cap Cameroon (C3)	Limbe (C2)	Rio del rey (C1)
1986-1994	-0.42	<b>0.52</b>	<b>0.52</b>	<b>0.51</b>	<b>0.5</b>
1995-2005	0.39	-0.39	0.07	0.29	0.05
2005-2020	-0.42	<b>0.5</b>	<b>-0.65</b>	0.35	-0.32

### 3.5 Spatial and temporal patterns in shoreline variability

An analysis of localized variability shows a dis-proportionality from one area to another. Taking into account the local characteristics (nature of the coastal substrate) allows to highlight the influence of waves on the morphological configuration of the coasts (Fig. 6a). However, the trend is reversed when we move to large time scales from 2012 onwards (Fig. 6b). This observation is even more evident on 10-year time scales (Fig. 6b). Fig. 6b shows two periods with erosive dominance regardless of the time scale of observation (C1 and C3). On the other hand, the Kribi zone experienced a first period (1992-2000) during which its northern part was slightly eroded, followed by a second period (2013-2019) with a

1 369 migration and enlargement of the eroded zone and a concentration of an accumulation zone  
2  
3  
4 370 further south (Fig. 6a and Fig. 2 a and b).

5  
6 371 Zone C2, for its part, is characterized by relative overall stability, although  
7  
8  
9 372 accompanied by regressive instability during 1991 and 2004, a period during which  
10  
11 373 maximum variations in wave height were observed.

12  
13 374 Part C3 (Cape Cameroon) experienced regressive coastline migration for nearly two  
14  
15  
16 375 decades (1986 - 2004). The variations observed in C3 during the 1986 - 2004 period were  
17  
18 376 accompanied by strong wave activity ( $1.35 \pm 0.4$  m), creating a significant trend in  
19  
20  
21 377 cumulative erosion estimated at around -10 m/year. A different dynamic emerges from  
22  
23 378 2007, characterized by a permanent stability until the end of the study. Less significant and  
24  
25  
26 379 almost uniform variations are observed in C4, with a progressive formation of a sandy spit.  
27  
28 380 The seasonal wave signal, although weak and permanent, is consistent with these slow  
29  
30  
31 381 changes (Fig. 4 - C4).

32  
33 382 To examine causal factors for spatial and temporal variations in more detail, an  
34  
35  
36 383 analysis of the empirical orthogonal function (EOF) of the generated shoreline change and  
37  
38 384 wave data was performed. The EOF analysis results show two modes (Fig. 6a) in each  
39  
40  
41 385 segment. Mode 1 accounts for 76.3% of the variability and mode 2 explains 23.7% of the  
42  
43 386 variability. Based on a similar study carried out in the Bight of Benin in West Africa (Anthony  
44  
45  
46 387 et al., 2019), mode 1 may be related to small scales associated with relatively pronounced  
47  
48 388 local erosion/accretion changes caused by natural shoreline dynamics, low angle of wave  
49  
50  
51 389 incidence at the point of surf ( $5^\circ - 10^\circ$ ) but also the presence of protective structures. Mode  
52  
53 390 2 can be interpreted as representing a larger scale associated with the progressive decrease  
54  
55  
56 391 in accretion from south to north over the study period (Fig. 6b), highlighting the influence of  
57  
58 392 regional-scale waves on coastline dynamics.

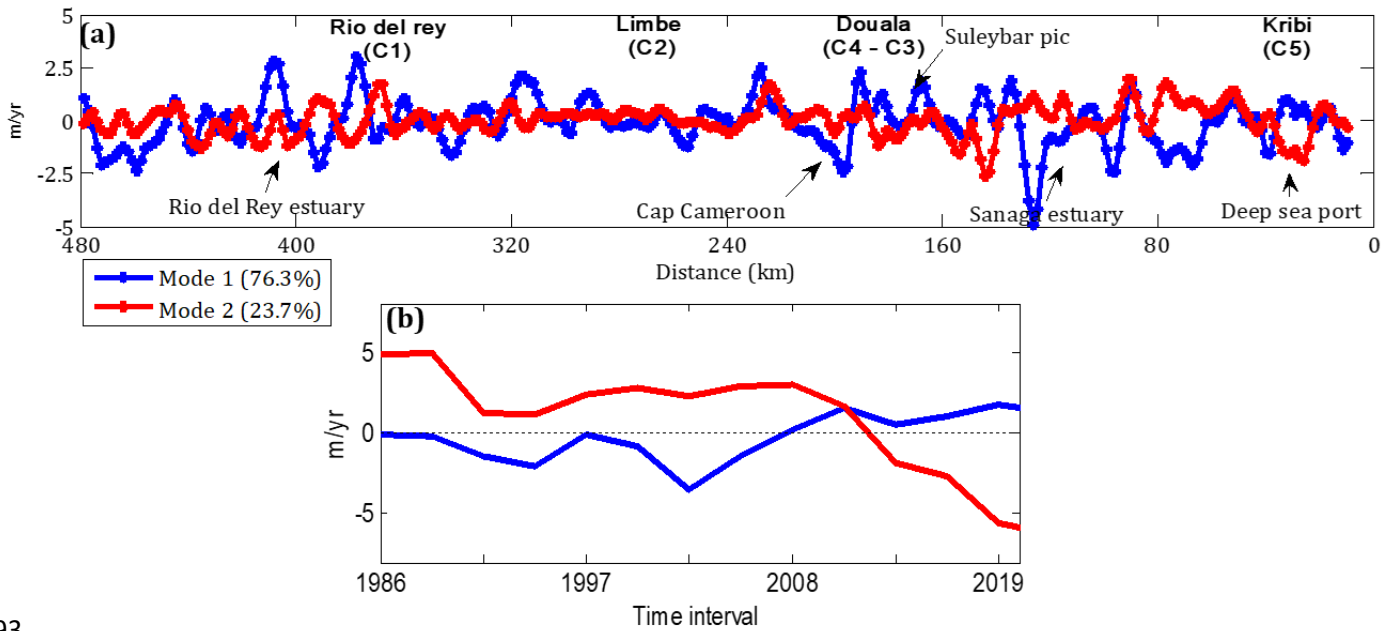


Figure 6 Maps of contributions to shoreline change: (a) Spatial mode EOF (mode1: 76.3% of total variance) and EOF2 (mode2: 23.7% of total variance); (b) Temporal mode expressing the temporal behaviour of the rate of change.

#### 4. Discussion

The decadal-scale analyses of changes of the Cameroonian coastline between 1986 and 2020 reveals on one hand a complex and segmented spatial configuration in five areas (C1 to C5) and on the other hand three temporal phases characterized by a significant fluctuation of the coastline with considerable variability between segments.

Estuaries are characterised by often complex dynamics as a result of interactions of river flow, waves, tides and coastal drift (Anthony et al., 2019; Abessolo et al., 2018; Dada et al., 2016). The strong erosion trends during the first period (1986-1994) in segments C1 and C3 are chiefly attributable to the cutting of mangroves amplified by an increase in sea level, and a resulting reduction in absorption of wave energy reaching the coast (Onguéné et al., 2015). Dada et al (2015) noted that shoreline retreat from the Niger Delta coastline, at a rate of 28 m/year, between 1950 and 1987 were mainly related to negative anomalies in rainfall

1 409 and river flows due to climate change. In addition, recent studies (e.g. Almar et al, 2015 ;  
2  
3  
4 410 Dada et al., 2015; Kuenzer et al., 2014; Obowu and Abam, 2014; Adegoke et al., 2010) have  
5  
6 411 suggested that the current coastline in West Africa alternates between erosion and accretion.  
7  
8  
9 412 Almar et al, 2015 demonstrated that this can be attributed to two distinct and simultaneous  
10  
11 413 processes: first order, the decrease in southwest swells generated by storms at mid-latitudes  
12  
13 414 and, second order, the increasing contribution of secondary swells southeast (which will  
14  
15  
16 415 cause coastal transport to the west, thereby reducing net coastal transport to the east)  
17  
18 416 generated by positive trade anomalies. However, it remains difficult to infer that the same  
19  
20  
21 417 processes affect the Cameroonian coast at the bottom of the bay of Bonny.

22  
23 418 The overall coastline displacement rate shows strong variations at the estuaries  
24  
25  
26 419 entrances (C1 and C3), as might be expected. A source of error could be due to the acquisition  
27  
28  
29 420 time of image-derived estuarine shorelines as the position of the sandbank depends on the  
30  
31 421 seasonal variability of river runoff and oceanic forcings (Onguéné, 2015). However,  
32  
33 422 cameroonian estuaries are characterized by the high flows of the Rio del rey rivers (C1), the  
34  
35  
36 423 Wouri estuary, one of the largest in the sub-region (C3 and C4), and the Sanaga river (Fig 2).  
37  
38 424 These regions have been identified as the main hot spots on the Cameroonian coast  
39  
40  
41 425 (Abessolo et al., 2018, Fossi et al., 2019). And the coastal currents in these estuaries have  
42  
43 426 been identified as responsible for the variability in sediment inputs that affect not only the  
44  
45  
46 427 dynamics of the coastline but also seasonal sediment transport. For example, the eroded area  
47  
48 428 of Cape Cameroon (C3) corresponds to the current flowing out of the estuary. Major port  
49  
50  
51 429 works or protection works, located on a coast affected by a predominantly coastal transit,  
52  
53 430 also disturb the balance of sediment transport, by blocking the materials on the "fed" face of  
54  
55  
56 431 the structures, they cause erosion under the "undernourished" face.

57  
58 432 Segments C2 and C4 (Limbé and Pointe de Souleyba) are characterized by moderate to  
59  
60  
61 433 significant accretion rates of 2.4 m/year and 18.5 m/year, dominated by natural shoreline

1 434 modification patterns, such as the Souleyba spit (C4) which is relatively recent feature.  
2  
3  
4 435 Abessolo et al. (2018) demonstrated that the convergence of the flows of the Wouri and the  
5  
6 436 Dibamba River associated with the littoral drift contribute to the accumulation of sediments  
7  
8  
9 437 observed at Souleyba (C4).. It is interesting to note that even if C4 integrates the shore  
10  
11 438 opposite to C3 in the mouth of the Wouri River, this side of the estuary corresponds to the  
12  
13 439 main source of sand supply from the shore in the estuary: the advance estimated at 69  
14  
15  
16 440 m/year in this sector was observed in the period 2010-2019 (Figure 3) and corresponds to  
17  
18 441 a convergence of sediments eroded on the southwestern part of Manoka Island and those  
19  
20  
21 442 sourced from the ocean. The rate of change of coastline displacement remains relatively  
22  
23 443 stable in section C2, as the lithological nature is characterized by the presence of cohesive  
24  
25  
26 444 sediments and rocky coasts as well as a coast dominated by the presence of mangroves and  
27  
28  
29 445 vegetation that absorb wave energy, which are otherwise very low in density in this segment.

30  
31 446 In the southern part C5, an abrupt change in dynamics is observed as of late 2012, likely  
32  
33 447 due to the construction of a 1.5 km offshore oriented dike at the port of Kribi (30 km to the  
34  
35  
36 448 south of Kribi) in late 2012. The amount of sediment bypassing the dike may not sufficient  
37  
38 449 to balance the high transport potential in this area (Fig. 2a, b). A number of quarries for  
39  
40  
41 450 extracting beach sand for construction purposes are located in the area, from which a volume  
42  
43 451 of more than 45,000 m<sup>3</sup>/year of sediment is extracted over the entire Kribi coastal strip  
44  
45  
46 452 (MINEPDED, 2017). The distance from the baseline (reference shoreline) shows fluctuating  
47  
48 453 displacements  $\pm 10$  m, especially between 2005 and 2020 (Fig. 2a). Such an alteration (with  
49  
50  
51 454 human intervention) of the balance between sediment input and coastal erosion leads to a  
52  
53 455 progressive degradation of the coastal system (Rovira and Ibàñez, 2007; Batalla et al., 2004;  
54  
55  
56 456 Sanchez-Arcilla et al., 1998).

57  
58 457 The interannual wave variability obtained in the present study shows a gradual  
59  
60  
61 458 increase in Hs since 1990. The order of magnitude of the increasing trends in mean Hs

1 459 (0.0017 to 0.003 m/year; Figure 5) found in the present study, particularly between 2005  
2  
3  
4 460 and 2020, are in line with the results of many studies carried out in the Gulf of Guinea sub-  
5  
6 461 region. Several ocean wave studies have reported an increase in Hs in the North Atlantic  
7  
8  
9 462 Ocean in recent decades (e.g. Bertin et al., 2013; Le Cozannet et al., 2011; Dodet et al., 2010).  
10  
11 463 Bertin et al. (2013) observed an increase in Hs over the entire North Atlantic Ocean based  
12  
13  
14 464 on numerical analysis of retrospective winds (1900 to 2008), reaching 0.01 m/yr and  
15  
16 465 gradually decreasing to less than 0.005 m/yr in the southern North Atlantic. The results  
17  
18  
19 466 obtained by Dada et al, 2016 in the coast of the Niger Delta (upper limit of Bonny Bay), are  
20  
21 467 slightly larger but of the same order of magnitude as that obtained in our study. This could  
22  
23  
24 468 be explained by the fact that the work of Dada et al. 2016 was calculated over a much longer  
25  
26 469 period (last 110 years) with a maximum increase in Hs of 0.0054 m/year. The seasonal  
27  
28  
29 470 rhythm of the coastline indicates a period of erosion corresponding to the passage of the  
30  
31 471 ITCZ over the equatorial zone characterized by heavy rainfall. During this period of heavy  
32  
33  
34 472 agitation (May to September), wave heights increase and the coast undergoes significant  
35  
36 473 disturbance. Almar et al. in 2015 demonstrated that the equatorial fluctuation of the  
37  
38  
39 474 Intertropical Convergence Zone (ITCZ) explains most of the variability in wave-induced  
40  
41 475 transport but also the predominant influence of the Southern Annular Mode (SAM) on wave-  
42  
43 476 induced transport.

45  
46 477 The results of the analysis of EOF variability patterns of spatial-temporal shoreline  
47  
48 478 changes show two modes. The first represents the relatively marked local influence of  
49  
50  
51 479 natural dynamics such as waves, drift currents and river flows at C1 (Rio del rey), C2 and C3  
52  
53  
54 480 (Wouri estuary) and along the coasts with the presence of coastal infrastructures, such as at  
55  
56 481 C5 (Fig 6a). The second mode represents larger scale changes. These results mainly show  
57  
58 482 that the changes on this coast are due to several factors, and that the wave regime acts in  
59  
60  
61 483 combination with several other factors at the local and regional level.

## 5. Conclusion

The evolution of the coastline based on a 34-year time series (1986 to 2020) of satellite image data (Earth Explorer and GEE) and the Era-interim re-analysed wave data improved the understanding of coastline variability and local and regional wave climate in the study area. The shoreline change analysis undertaken here reveals a permanent and localized erosive trend on two segments (C1 and C3) over the 402 km along the Cameroonian coast. Nevertheless, a seasonal signal on coastline variability is evident, corroborated by the strong interannual variability in local and regional wave climate. The EOF analysis has highlighted two modes of variability representing respectively the local spatiotemporal scale influence mode 1, but also a larger scale influence mode 2. While this study suggests that shoreline changes are strongly related to local and regional wave climate variability, it is important to note that shoreline stability is also strongly dependent on a constant supply of sediments, and other processes such as: variability of river flows in drift currents, and anthropogenic effects, may act in combination with changes in wave regime and resulting coastal transport to influence shoreline changes along the Cameroonian coast.

## Acknowledgements

This project was funded by the *service de coopération et d'Action Culturelle* (SCAC) of the French Embassy in Cameroon within the framework of a research mobility grant awarded to Njutapvoui Nourdi, as part of a co-supervision agreement between the University of Douala (UDo\_EDSFA) and the University Paris Est Marne la Vallée. We used data provided through the ECMWF ERA Interim dataset ([www.ECMWF.Int/research/Era](http://www.ECMWF.Int/research/Era)), Landsat images downloaded from [earthexplorer.usgs.gov](http://earthexplorer.usgs.gov), Google Earth Engine (GEE) and Sentinel images from the ESA Copernicus program (<https://scihub.copernicus.eu/dhus/>).

## References

- Abessolo Ondo, G.; Onguéné, R.; Tomedi Eyango, M.; Duhaut, T.; Mama, C.; Angnuureng, B.D., and Almar, R., 2018. Assessment of the evolution of Cameroon coastline: An overview from 1986 to 2015. *In: Tropical Coastal and Estuarine Dynamics. Journal of Coastal Research*, Special Issue, No. 81, pp. 122–129. Coconut Creek (Florida), ISSN 0749-0208.
- Adams, P.N., Inman, D.L., Lovering, J.L., 2011. Effects of climate change and wave direction on longshore sediment transport patterns in Southern California. *Clim. Chang.* 109, 211–228.
- Adegoke, J.O., Fageja, M., Godstime, J., Agbaje, G., Ologunorisa, T.E., 2010. An assessment of recent changes in the Niger Delta coastline using satellite imagery. *J. Sustain. Dev.* 3(4), 277–296.
- Ajonina, G.N., 2010. Rapport final de réalisation du mandat. Consultation Project GEF PPG, 36p.
- Almar, R.; Honkonnou, N.; Anthony, E.J.; Castelle, B.; Senechal, N.; Laibi, R.; Mensah-Senoo, T.; Degbe, G.; Quenum, M.; Dorel, M.; Chuchla, R.; Lefebvre, J. P.; Du Penhoat, Y.; Laryea, W. S.; Zodehougan, G.; Sohoun, Z.; Addo, K.A.; Ibaceta, R., and Kestenare, E., 2014. The Grand Popo beach 2013 experiment, Benin, West Africa: From short timescale processes to their integrated impact over long-term coastal evolution. *In: Green, A.N. and Cooper, J.A.G. (eds), Proceedings 13th International Coastal Symposium (Durban, South Africa). Journal of Coastal Research*, Special Issue No. 70, pp. 651-656.
- Almar, R.; Kestenare, E.; Reyns, J.; Jouanno, J.; Anthony, E.J.; Laibi, R.; Hemer, M.; Du Penhoat, Y., and Ranasinghe, R., 2015. Response of the Bight of Benin (Gulf of Guinea, West Africa) coastline to anthropogenic and natural forcing, Part1: Wave climate variability and impacts on the longshore sediment transport. *Continental Shelf Research*, 110, 48-59.
- Angnuureng, D. B., R. Almar, K. Appeaning Addo, N. Senechal, B. 438 Castelle, S.W. Laryea, and G. Wiafe, 2016: Video observation of waves and shoreline change on the microtidal

1 532 James town Beach in Ghana. *Journal of Coastal Research, Proceedings of the 14th*  
2  
3  
4 533 *International Coastal Symposium, Sydney, Australia, Special Issue 75, 1022 – 1026, ISSN*  
5  
6 534 0749-0208.

7  
8  
9 535 Anthony .E.J., R. Almar., M. Besset., J. Reyns., R. Laibi., R. Ranasinghe., G. Abessolo Ondo., M.  
10  
11 536 Vacchi; 2019 : Response of the Bight of Benin (Gulf of Guinea, West Africa) coastline to  
12  
13 537 anthropogenic and natural forcing, Part 2: Sources and patterns of sediment supply,  
14  
15  
16 538 sediment cells, and recent shoreline change. *Continental Shelf Research* 173 (2019) 93–  
17  
18 539 103 (<https://doi.org/10.1016/j.csr.2018.12.006>)

20  
21 540 Anthony, E.J., 2017. Beach erosion. In: Finkl, C., Makowski, C. (Eds.), *Encyclopedia of Coastal*  
22  
23 541 *Science. Encyclopedia of Earth Sciences Series. Springer, Cham.*

24  
25  
26 542 Batalla, R.J., Gomez, C.M., Kondolf G. M., 2004. Reservoir-induced hydrological changes in the  
27  
28 543 Ebro River basin (NE Spain). *J. Hydrol.* 290, 117–136.

29  
30  
31 544 Battjes, J.A.; Janssen, J.P.F.M. Energy loss and setup due to breaking of random waves. In  
32  
33 545 *Proceedings of the ASCE International Conference on Coastal Engineering, Hamburg,*  
34  
35  
36 546 *Germany, 27 August–3 September 1978; pp. 569–587.*

37  
38 547 Bertin, X., Prouteau, E., Letetrel, C., 2013. [A significant increase inwave height in the North](#)  
39  
40  
41 548 [Atlantic Ocean over the 20th century. \*Glob. Planet. Chang.\* 106, 77.](#)

42  
43 549 Boateng, I., 2009. Development of integrated shoreline management planning: A case study  
44  
45 550 of keta, Ghana. *TS 4E—Coastal Zone Management. FIG Working Week 2009. Surveyors*  
46  
47  
48 551 *Key Role in Accelerated Development Eilat, Israel, 3–8 May 2009.*

49  
50  
51 552 Boateng, I., 2012. An application of GIS and coastal geomorphology for large scale assessment  
52  
53 553 of coastal erosion and management: a case study of Ghana. *J. Coast. Conserv.* (16), 383–  
54  
55  
56 554 397. <http://dx.doi.org/10.1007/s11852-012-0209-0>.

57  
58  
59  
60  
61  
62  
63  
64  
65

1 555 Bosom, E. and Jiménez, J.A., 2011. Probabilistic coastal vulnerability assessment to storms at  
2  
3  
4 556 regional scale - application to Catalan beaches (NW Mediterranean). *Natural Hazards and*  
5  
6 557 *Earth System Science*, 11, 475–484.  
7  
8  
9 558 Caires S, Swail VR, Wang XL., 2006 Projection and analysis of extreme wave climate. *J Clim*  
10  
11 559 19:5581–5605  
12  
13 560 Dada, O.A., Qiao, L.L., Ding, D., Li, G.X., Ma, Y.Y., Wang, L.M., 2015. Evolutionary trends of the  
14  
15  
16 561 Niger Delta Shoreline during the last 100 years: responses to rainfall and river  
17  
18 562 discharge. *Mar. Geol.* 367, 202–211. <http://dx.doi.org/10.1016/j.margeo.2015.06.007>.  
19  
20  
21 563 Dada, O. A., Li, G., Qiao, L., Ma, Y., Ding, D., Xu, J., ... Yang, J. (2016). *Response of waves and*  
22  
23 564 *coastline evolution to climate variability off the Niger Delta coast during the past 110years.*  
24  
25  
26 565 *Journal of Marine Systems*, 160, 64–80. doi:10.1016/j.jmarsys.2016.04.005  
27  
28  
29 566 Dee, D.P.; Uppala, S.M.; Simmons, A.J.; Berrisford, P.; Poli, P.; Kobayashi, S.; Andrae, U.;  
30  
31 567 Balmaseda, M.A.; Balsamo, G.; Bauer, P.; Bechtold, P.; Beljaars, A.; Van De Berg, L.;  
32  
33 568 Bidlot, J.R.; Bormann, N.; Delsol, C.; Dragani, R.; Fuentes, M.; Geer, A.J.; Haimberger, L.;  
34  
35  
36 569 Healy, S.; Hersbach, H.; Hólm, E.V.; Isaksen, I.; Kållberg, P.W.; Köhler, M.; Matricardi, M.;  
37  
38 570 McNally, A.; Monge-Sanz, B.M.; Morcrette, J.J.; Peubey, C.; De Rosnay, P.; Tavolato, C.;  
39  
40  
41 571 Thépaut, J.N., and Vitart, F., 2011. The ERA-Interim reanalysis: Configuration and  
42  
43 572 performance of the data assimilation system. *Quarterly Journal of the Royal Meteorological*  
44  
45  
46 573 *Society*, 137(656), 553-597.  
47  
48 574 Dodet, G., Bertin, X., Taborda, R., 2010. [Wave climate variability in the North East Atlantic](#)  
49  
50  
51 575 [over the last 6 decades.](#) *Ocean Model.* 31, 120–131  
52  
53 576 Faye, I.B.N., 2010. Dynamique du trait de côte sur les littoraux sableux de la Mauritanie à la  
54  
55  
56 577 Guinée-Bissau (Afrique de l'Ouest) : Approches régionale et locale par photo-  
57  
58 578 interprétation, traitement d'images et analyse de cartes anciennes ». Volume 1, thèse de  
59  
60  
61 579 doctorat, *Géographie*, Université de Bretagne Occidentale, 321p.  
62  
63  
64  
65

1 580 Fernand Verger, Raymond Ghirardi et al., 2002 *L'espace nouveau territoire : Atlas des*  
2  
3  
4 581 *satellites et des politiques spatiales*, Paris, Belin, 383 p. ([ISBN 978-2-701-13194-8](#) et [2-](#)  
5  
6 582 [701-13194-4](#), [OCLC 51653010](#))  
7  
8  
9 583 Fotsi, Pouvreau, Brenon, Onguene, & Etame. (2019). *Temporal (1948–2012) and Dynamic*  
10  
11 584 *Evolution of the Wouri Estuary Coastline within the Gulf of Guinea. Journal of Marine Science*  
12  
13 585 *and Engineering*, 7(10), 343. doi:10.3390/jmse7100343  
14  
15  
16 586 Giardino, A., Schrijvershofa, R., Nederhoffa, C.M., de Vroega, H., Brièrea, C., Tonnona, P.-K.,  
17  
18 587 Cairesa, S., Walstraa, D.J., Sosac, J., van Versevela, W., Schellekensa, J., Sloffa, C.J., 2018. A  
19  
20  
21 588 quantitative assessment of human interventions and climate change on the West African  
22  
23 589 sediment budget. *Ocean Coast. Manag.* 156, 249–265.  
24  
25  
26 590 Giresse, P.; Megope, F.J.; Ngueutchoua, G., and Aloisi, J.C.,1996. *Carte Sédimentologique du*  
27  
28 591 *Plateau Continental du Cameroun*. Paris, France: ORSTOM, *Collection Notice Explicative N°*  
29  
30 592 *111*, 12p.  
31  
32  
33 593 Hapke, C.J., Himmelstoss, E.A., Kratzmann, M., List, J.H., Thieler, E.R., 2010. National  
34  
35  
36 594 assessment of shoreline change: Historical shoreline change along the New England and  
37  
38 595 Mid-Atlantic coasts: US Geological Survey Open-File Report 2010-1118. p. 57.  
39  
40  
41 596 Kuenzer, C., van Beijma, S., Gessner, U., Dech, S., 2014. Land surface dynamics and  
42  
43 597 environmental challenges of the Niger Delta, Africa: remote sensing-based analyses  
44  
45  
46 598 spanning three decades (1986-2013). *Appl. Geogr.* 53, 354–368.  
47  
48  
49 599 Laibi, R.A., Anthony, E.J., Almar, N., Castelle, B., Sénéchal, Kestenare, E., 2014. Longshore drift  
50  
51 600 cell development on the human-impacted Bight of Benin sand barrier coast, West Africa.  
52  
53 601 *J. Coast. Res.* (Special 70), pp.78–83.  
54  
55  
56 602 Larson M, Hoan L, Hanson H. 2010 Direct formula to compute wave height and angle at  
57  
58 603 incipient breaking. *J Waterway Port Coast Ocean Eng* 136:119–122  
59  
60  
61  
62  
63  
64  
65

1 604 Le Cozannet, G., Lecacheux, S., Delvallee, E., Desramaut, N., Oliveros, C., Pedreros, R., 2011.  
2  
3 605 [Teleconnection pattern influence on sea-wave climate in the Bay of Biscay](#). *J. Clim.* 24 (3),  
4  
5  
6 606 641–652.  
7  
8 607 Luijendijk, A., Hagenaars, G., Ranasinghe, R., Baart, F., Donchyts, G., Aarninkhof, S., 2018. The  
9  
10  
11 608 state of the world’s beaches. *Sci. Rep.* 1–11. [https://doi.org/10.1038/s41](https://doi.org/10.1038/s41598-018-24630-6)  
12  
13 609 24630-6.  
14  
15 610 Longuet-Higgins, M.S., 1970. Longshore currents generated by obliquely incident sea  
16  
17  
18 611 waves: 1. *J. Geophys. Res.* 75, 6778–6789. <http://dx.doi.org/10.1029/JC075i033p06778>.  
19  
20  
21 612 Melet, A.; Almar, R., and Meyssignac, B., 2016. What dominates sea level at the coast: A case  
22  
23 613 study for the Gulf of Guinea. *Ocean Dynamics*, 66, 623-636.  
24  
25 614 Melet, A., B. Meyssignac, R. Almar, and G. Le Cozannet, 2018: Under-estimated wave  
26  
27  
28 615 contribution to coastal sea-level rise. *Nature Climate Change*,  
29  
30  
31 616 <https://doi.org/10.1038/s41558-018-0088-y>.  
32  
33 617 MINEPDED-RCM, 2017 : Etat des lieux des mangroves du Cameroun. Ministère de  
34  
35  
36 618 l’Environnement, de la Protection de la Nature et du Développement Durable en  
37  
38 619 collaboration avec le Réseau Camerounais des Mangroves. P.10-11. Juin 2017  
39  
40  
41 620 Moore L. J., Griggs G.B. 2002 Long-term cliff retreat and erosion hotspots along the central  
42  
43 621 shores of the Monterey Bay National Marine Sanctuary. *Marine Geology*, vol. 181, n°1-3, p.  
44  
45  
46 622 265 - 283.  
47  
48 623 Obowu, C.D., Abam, T.K.S., 2014. Spatial and multi-temporal change analysis of the Niger  
49  
50  
51 624 Delta coastline using remote sensing and geographic information system (GIS). *Int. J.*  
52  
53 625 *Remote Sensing Appl.* 4 (1), 41–47.  
54  
55 626 ONEQUIP, 2009 – Contrat N° 01090031 relatif à l’élaboration d’un programme de suivi de la  
56  
57  
58 627 vitalité des mangroves camerounaises. Projet CAPECE-CPSP/SNH. Rapport final, 146p.  
59  
60  
61  
62  
63  
64  
65

- 1 628 Onguéné, R., 2015. Modélisation Multi-Echelles de la Circulation Océanique en Afrique  
2  
3  
4 629 Centrale, de la Plaine Abyssale à l'Estuaire du Cameroun. Toulouse, France: University of  
5  
6 630 Toulouse III Paul Sabatier, Ph.D. dissertation, 216p.  
7  
8  
9 631 Onguene, R., *et al.* (2015) Overview of Tide Characteristics in Cameroon Coastal Areas Using  
10  
11 632 Recent Observations. *Open Journal of Marine Science*, **5**, 81-98.  
12  
13 633 <http://dx.doi.org/10.4236/ojms.2015.51008>  
14  
15  
16 634 Pilkey, O.H., Cooper, J.A.G., 2014. Are natural beaches facing extinction? *J. Coast. Res.* 70, 78–  
17  
18 635 83.  
19  
20  
21 636 Ranasinghe, R., 2016. Assessing climate change impacts on open sandy coasts: A review,  
22  
23 637 *Earth-Science Reviews*, 160, 320–332, doi:10.1016/j.earscirev.2016.07.011.  
24  
25  
26 638 Richards, J. and Nicholls, R.J., 2009. *Impacts of Climate Change in Coastal Systems in Europe.*  
27  
28 639 *PESETA Coastal Systems study*. Luxembourg: European Commission, Joint Research  
29  
30 640 Center. *JRC Scientific and Technical Reports, JRC 55390, EUR 24130 EN*.  
31  
32  
33 641 Rovira, A., Ibàñez, C., 2007. Sediment management options for the lower Ebro River and its  
34  
35 642 Delta. *J. Soils Sediment.* 7(5), 285–295.  
36  
37  
38 643 Robin, M., 2002. Télédétection et modélisation du trait de côte et de sa cinématique. *In*  
39  
40 644 (Baron-Yelles N. Goeldner-Gionella L., Velut S., Ed.) *Le littoral, regards, pratiques et savoirs.*  
41  
42 645 *Etudes offertes à Fernand VERGER*. Edition Rue d'Ulm / Presses universitaires de l'Ecole  
43  
44 646 Normale Supérieure, Paris, p. 95 - 115.  
45  
46  
47  
48 647 Sanchez-Arcilla, A., Jimenez, J. A., Valdemoro, H. I., 1998. The Ebro Delta: morphodynamics  
49  
50 648 and vulnerability. *J. Coast. Res.* 14(3), 754–772.  
51  
52  
53 649 Stafford D.B., Langfelder J. 1971 Air photo survey of coastal erosion. *Photogrammetric*  
54  
55 650 *Engineering*, vol. 37, p. 565 - 575.  
56  
57  
58 651 Sterl, A. and Caires, S., 2005. Climatology, variability and extrema of ocean waves- the web-  
59  
60 652 based KNMI/ERA-40 wave atlas. *International Journal of Climatology*, 25, 963–977.  
61  
62  
63  
64  
65

1 653 Tano, R.A.; Aman, A.; Kouadio, K.Y.; Toualy, E.; Ali, K.E., and Assamoi, P., 2016. Assessment of  
2  
3  
4 654 the Ivorian Coastal Vulnerability. *Journal of Coastal Research*, 32(6), 1495– 1503  
5  
6 655 Thieler, E.R., Himmelstoss, E.A., Zichichi, J.L., Ergul, A., 2009. The Digital Shoreline Analysis  
7  
8  
9 656 System (DSAS) version 4.0an ArcGIS Extension for Calculating Shoreline Change.  
10  
11 657 Available at: <<http://woodshole.er.usgs.gov/project-pages/DSAS/version4/index.html>>.  
12  
13  
14 658 Van der Walt, S., Scheonberger, J.L., Nunez-Iglesias, J., Boulogne, F., Warner, J.D., Yager, N.,  
15  
16 659 Gouillart, E., Yu, T., 2014. scikit-image : image processing in Python. *PeerJ* 2, e453.  
17  
18 660 <https://doi.org/10.7717/peerj.453>.  
19  
20  
21 661 Vos, K., Splinter, K. D., Harley, M. D., Simmons, J. A., & Turner, I. L. (2019). *CoastSat: A Google*  
22  
23 662 *Earth Engine-enabled Python toolkit to extract shorelines from publicly available satellite*  
24  
25  
26 663 *imagery. Environmental Modelling & Software,*  
27  
28 664 *104528. doi:10.1016/j.envsoft.2019.104528*  
29  
30  
31 665 Vos, K., Harley, M.D., Splinter, K.D., Simmons, J.A., Turner, I.L., 2019. Sub-annual to multi-  
32  
33 666 decadal shoreline variability from publicly available satellite imagery. *Coast. Eng.* 150,  
34  
35  
36 667 160–174. <https://doi.org/10.1016/j.coastaleng.2019.04.004>.  
37  
38 668 <https://earthexplorer.usgs.gov/>  
39  
40  
41 669 <https://scihub.copernicus.eu/dhus/>  
42  
43 670 <https://apps.ecmwf.int/datasets/data/interim-full-daily/>  
44  
45  
46  
47  
48  
49  
50  
51  
52  
53  
54  
55  
56  
57  
58  
59  
60  
61  
62  
63  
64  
65

**Conflicts of Interest:** The authors declare no conflict of interest.